ORIGINAL RESEARCH ARTICLE

Effect of Temperature and Stress on Hot Impression Creep Behavior of Cu-1.5 Zn Alloy

C. Vanitha, Baro Kaushik, and C. Sashank

Cu-1.5 wt.% Zn alloy used in the present study was subjected to the hot impression creep tests at three stresses of 75, 110 and 150 MPa and three temperatures of 250, 300 and 350 °C for a constant dwell time of 2 h. The effect of stress and temperature on the impression depth with respect to time was studied. Irrespective of the test condition, the depth of impression increased with respect to the time. However, upon increasing the applied stress, the twins were observed. Stress exponent values and activation energies were determined for different test temperatures and stresses. Stress exponent values related to the plastic flow over the complete range of experimental conditions were found to lie between 4 and 5.5. Whereas the average activation energy value was determined to be 164 ± 10 kJ/mol. Calculated stress exponents and activation energy values reveal the dislocation climb phenomenon, controlled by dislocation pipe diffusion as the mechanism of the creep.

1. Introduction

Pure copper has been widely used in the electrical and electronic industries because of its high thermal and electrical conductivity (Ref 1). Hence, it is a perfect material of choice for power and telecommunications cables, winding wires in electric motors, and a variety of other electrical applications (Ref 2). Pure copper provides good mechanical properties for applications up to a temperature of 100 °C, beyond which these properties start deteriorating (Ref 3). Copper alloys with Zn, Fe, Al, etc., could retain the mechanical properties at high temperatures by virtue of retaining its FCC crystal structure (Ref 3). But it has been noted that in several electronic devices with Cu alloys as wires or connects, upon increasing the density of component and decreasing the wire width, the temperature in

electronic devices might reach to values of around 200 to 300 °C (Ref 4, 5). Since these Cu-Zn alloys are being used at high temperatures and are subjected to stresses, creep study of these alloys is highly crucial in order to predict material failure (Ref 6, 7). Among different creep testing methods, impression creep test finds itself a special place as it offers highly localized creep information for a wide range of materials when compared to burdensome traditional creep tests (Ref 8-12).

Kuchařová et al. investigated creep in a Cu-2Fe alloy in the temperature domain of 673–873 K and the stress range of 10–95 MPa. It was found that the Coble diffusion deformation mechanism dominated at low stresses. Whereas, at high stresses, the steady state creep mechanism was controlled by the new interface area created during thermally assisted cutting of coherent γ iron particles present in the alloy (Ref 13).

Fakhrabadi et al. studied the impression creep behavior of the aged Cu-6Ni-2Mn-2Sn-2Al alloy in the temperature domain of 695-795 K at impression stresses in the range of 300-900 MPa. The average values of stress exponent and activation energy obtained were 4 and 194 kJ/mol, respectively. Dislocation climb controlled by lattice diffusion was found to be the responsible creep mechanism. It was also found that separately adding of 0.3 wt.% Cr and 0.3 wt.% Zr to the base alloy resulted in an even greater improvement in creep resistance (Ref 14).

Mahmudi et al. investigated the impression creep behavior of Cu-0.3Cr-0.1Ag alloy in the temperature range of 688-855 K for which the stress range of 80-550 MPa was used. It was found that Cu and Ag enhanced the creep resistance. It was also found that the creep mechanism was dislocation climb controlled by dislocation pipe diffusion (Ref 15). Further, it was also demonstrated that the punching stress required to obtain the same impression creep rate in Cu-0.3Cr-0.1Ag alloy was nearly 3 times the same as required in Cu. This increase in the punching stress required can be attributed to the strengthening effect caused by dispersion of Cr particles in the Cu matrix (Ref 16).

C. Vanitha, Baro Kaushik, and **C. Sashank**, Department of Metallurgical and Materials Engineering, National Institute of Technology Warangal, Hanamkonda, Telangana, India. Contact e-mail: vanitha@nitw.ac.in.

Kumar et al. have studied the effect of temperature and load during hot impression creep of Cu-Zn-Al alloy using 2, 2.5, and 3 kg load at 250, 300 and 350 °C. It was observed that both the impression depth and creep rate increased with an increase in

Fig. 1 OM image of as-received Cu-1.5 Zn alloy showing the presence of non-equiaxed grains and several twins

Table 1 Chemical Composition of Cu-1.5 Zn alloy

Elements	Cu	Zn
Wt.%	98.5	1.5

temperature as well as the load. The presence of several deformation bands upon increasing the stress was also distinctly revealed in their studies (Ref 17).

However, most of the existing literature neither paid close attention to impression creep studies on Cu-Zn alloys nor the microstructural changes occurring in the impression zone after. Hence, in the current work, creep properties of Cu-1.5 Zn alloy have been studied by the hot impression creep method due to the plethora of advantages it has over the conventional creep test (Ref 18, 19). The microstructural changes occurring in the vicinity of the impression zone have been carefully examined and it has been effectively correlated with the obtained creep properties. Additionally, efforts have been taken to determine the creep-controlling mechanism in Cu-1.5 Zn alloy at temperature and stress ranges of 250 to 350 °C and 75 to 150 MPa, respectively.
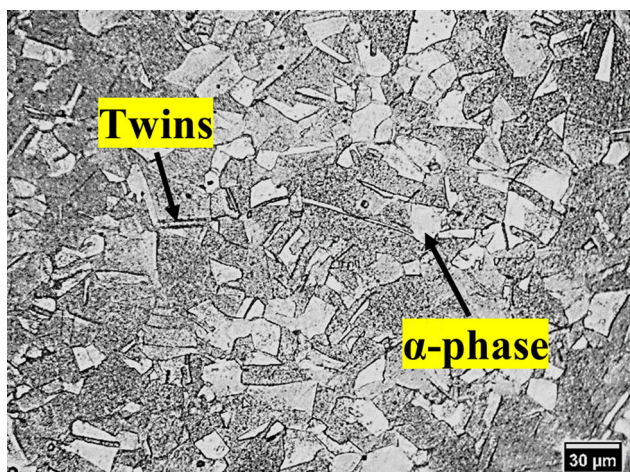
2. Experimental Procedure

2.1 Material

The as-received sample of Cu-1.5 Zn alloy in the annealed conditions were machined to dimensions of 15 mm diameter and 10 mm height. The Chemical composition determined through X-ray Fluorescence (XRF) analysis is described in Table 1.
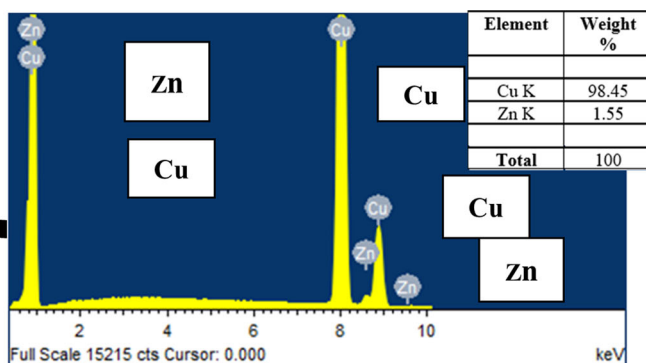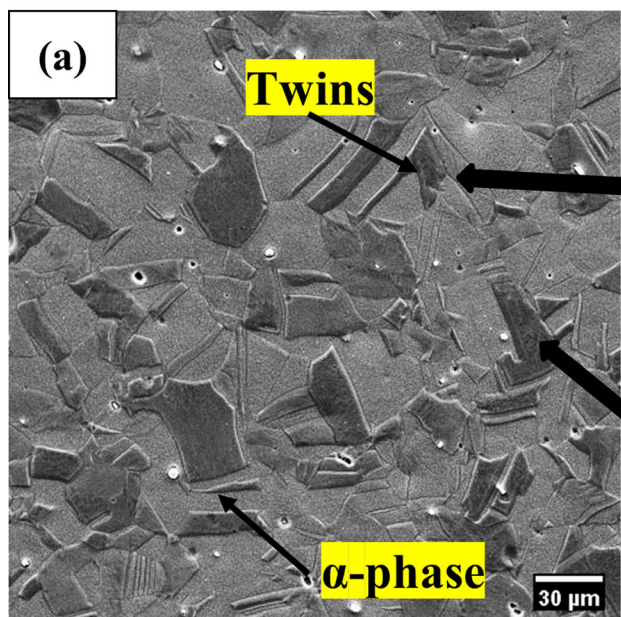
2.2 Metallography

The cylindrical samples were polished, adopting the standard metallographic polishing method and were then etched
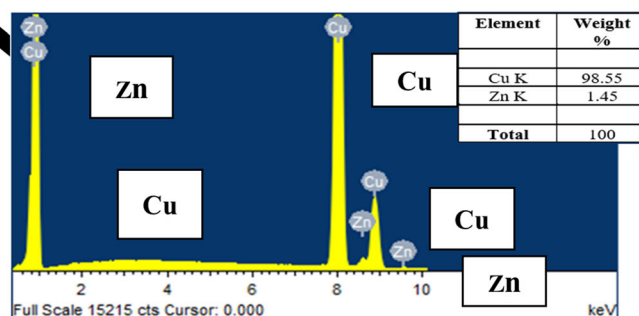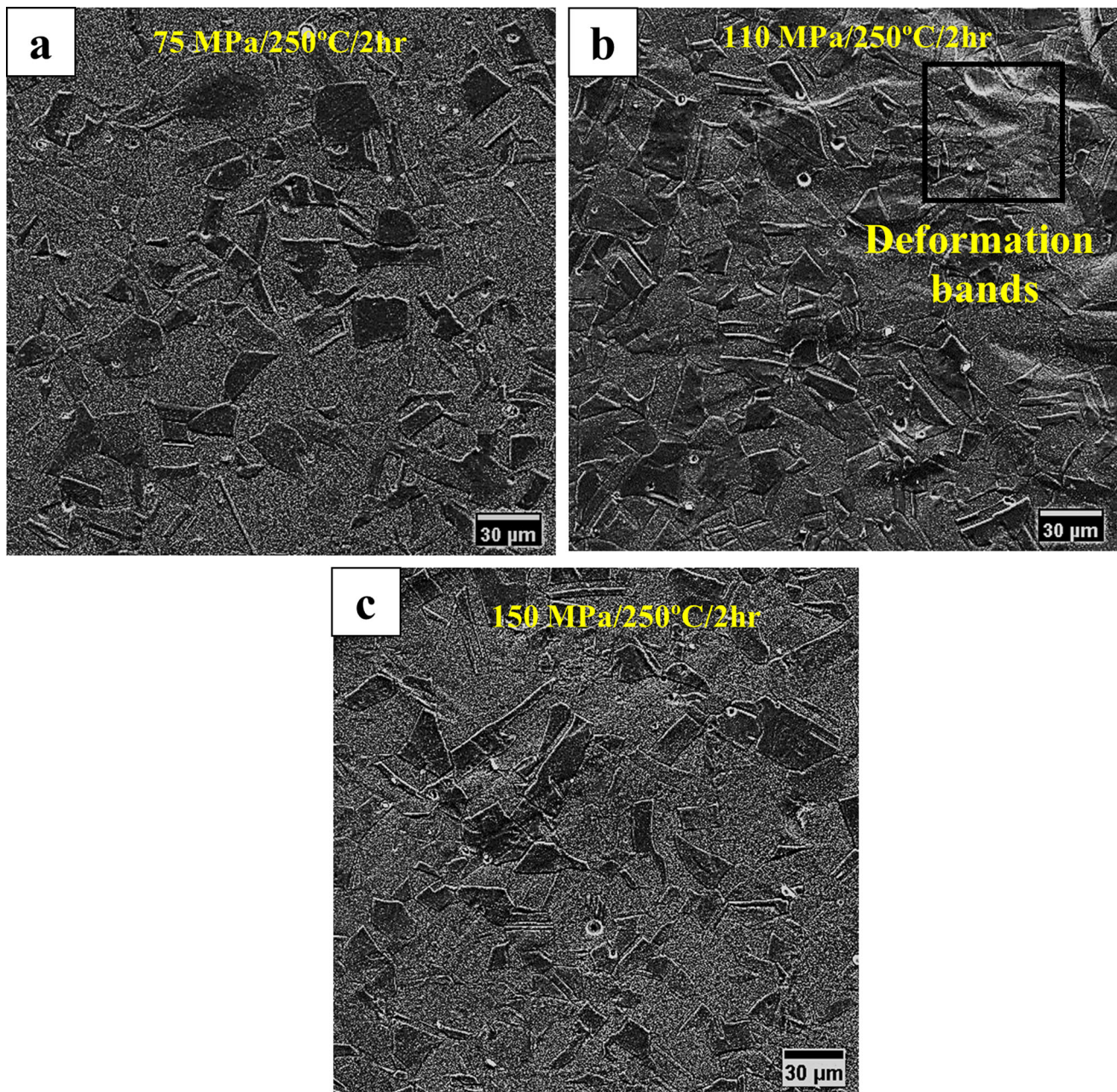

Fig. 2 (a). SEM image of as-received Cu-1.5 Zn alloy, (b) EDS of the bright region and (c) EDS of the dark reg

Fig. 3 SEM images of the impression region of Cu-1.5 Zn samples tested at 250ºC and load (a) 75 MPa (b) 110 MPa (c) 150 MPa

using a mixture of 25 ml HNO_3 and 25 ml distilled water for 40 seconds and then examined under a scanning electron microscope (Tescan-Vega3LMU). EDS was used to measure the chemical composition.

2.3 Hot impression Creep Test

The samples were tested at three different temperatures of 250, 300 and 350 °C and three different loading conditions of 75, 110 and 150 MPa for a dwell time of 2 h. Impression depth measured by the Linear Variable Displacement Transducer (LVDT) sensor was plotted with respect to time to get the depth of impression vs time plot. From this plot, several important data like steady-state creep rate, punch velocity vs time plot and steady-state punch velocity were obtained. In the secondary region within the creep curve, the relationship between steady-state punch velocity and impression stress is given by power law as given below:

$$\left(\frac{V_{imp} * T}{G}\right) = A\left(\frac{\sigma_{imp}}{G}\right)^n \exp\left(\frac{-Q}{RT}\right) \qquad \text{(Eq 1)}$$

where V_{imp} is the steady state punch velocity (m/s), G is the shear modulus (MPa), A is a material parameter, σ_{imp} is the impression stress (MPa), n is the stress exponent, Q is the activation energy (kJ/mol), T is the temperature (in K) and R is the universal gas constant (Ref 20).

At a constant T, the slope of the plot drawn between $\ln[V_{imp} * T/G]$ and $\ln[\sigma_{imp}/G]$ gives the value of stress exponent (n), since A is constant. Similarly, the slope of the curve obtained by plotting between 1000/T (where T is in K) and $\ln[V_{imp} * T/G]0.17em- n \ln[\sigma_{imp}/G]$ gives the value of
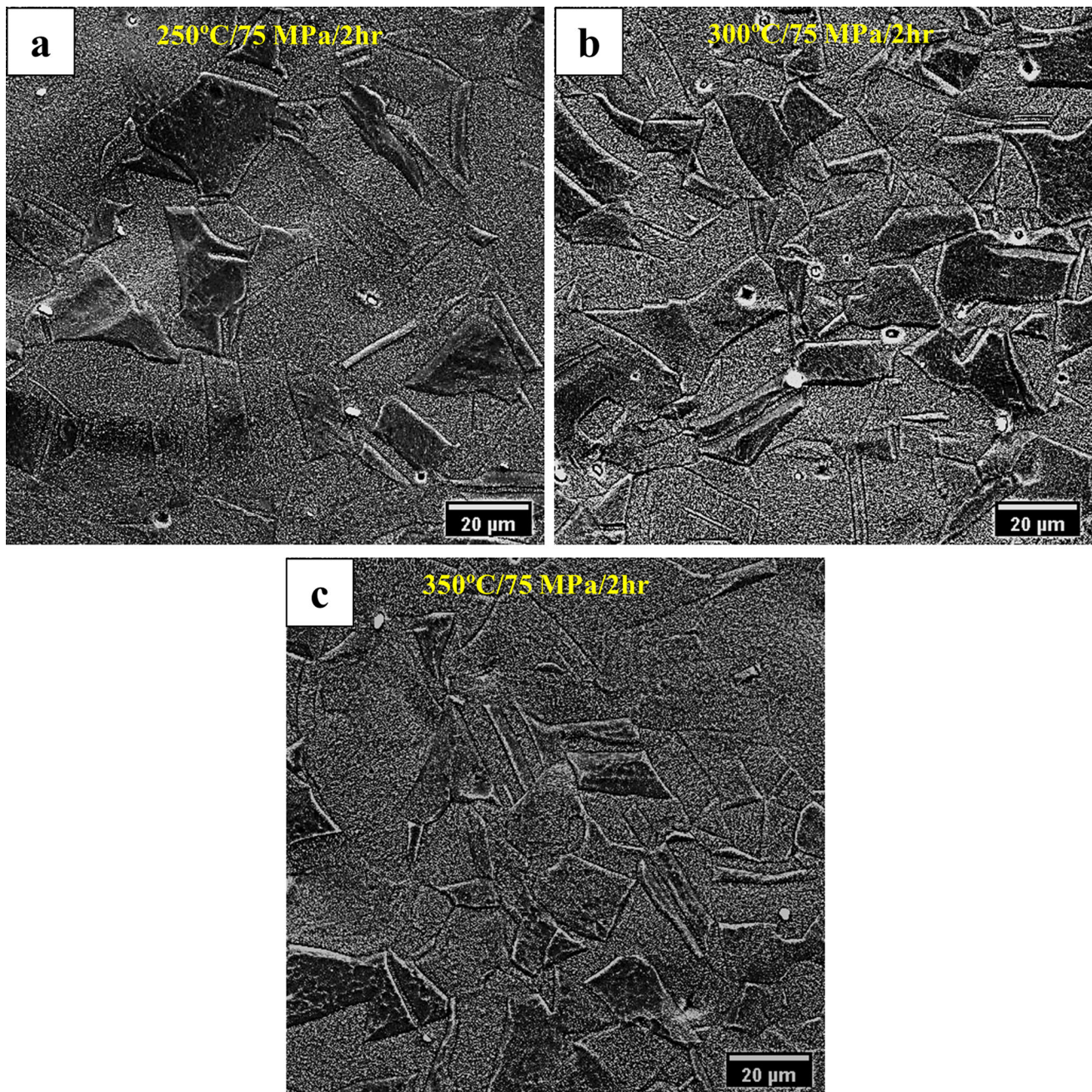
Fig. 4 SEM images of the impression region subjected to 75 MPa at different temperatures (a) 250ºC (b) 300ºC (c) 350ºC

$(-Q/R)$, from which the value of activation energy, Q can be found.

Since shear modulus of elasticity varies with testing temperature, the corresponding relationship which considers shear modulus as a function of temperature has to be utilized while calculating the values of n and Q. The following equation gives the value of shear modulus as a function of testing temperature for pure Cu. The temperature dependency of the elastic shear modulus of pure Cu can be applied to the present material under consideration.

$$G(\text{MPa}) = 47,500 - 17T(\text{K}) \qquad \text{(Eq 2)}$$

where G is the shear modulus (MPa) and T is the temperature (in K) (Ref 21).

3. Results and Discussion

3.1 Microstructural Features

Figure 1 depicts the Optical Microscope (OM) image of the Cu-1.5 Zn alloy in the as-received or annealed condition. From this image, it can be noted that the microstructure consists of single phase non-equiaxed α grains. Several annealing twins and twin boundaries were also present in the microstructure.
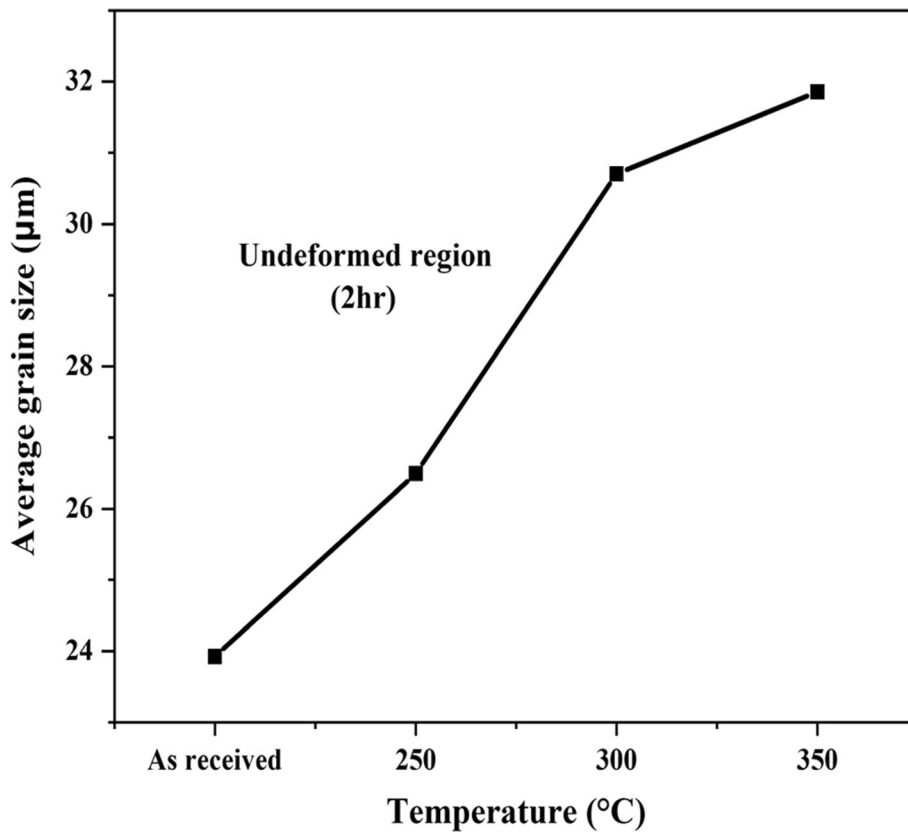
Fig. 5 Average grain size vs Temperature (ºC) in the undeformed region
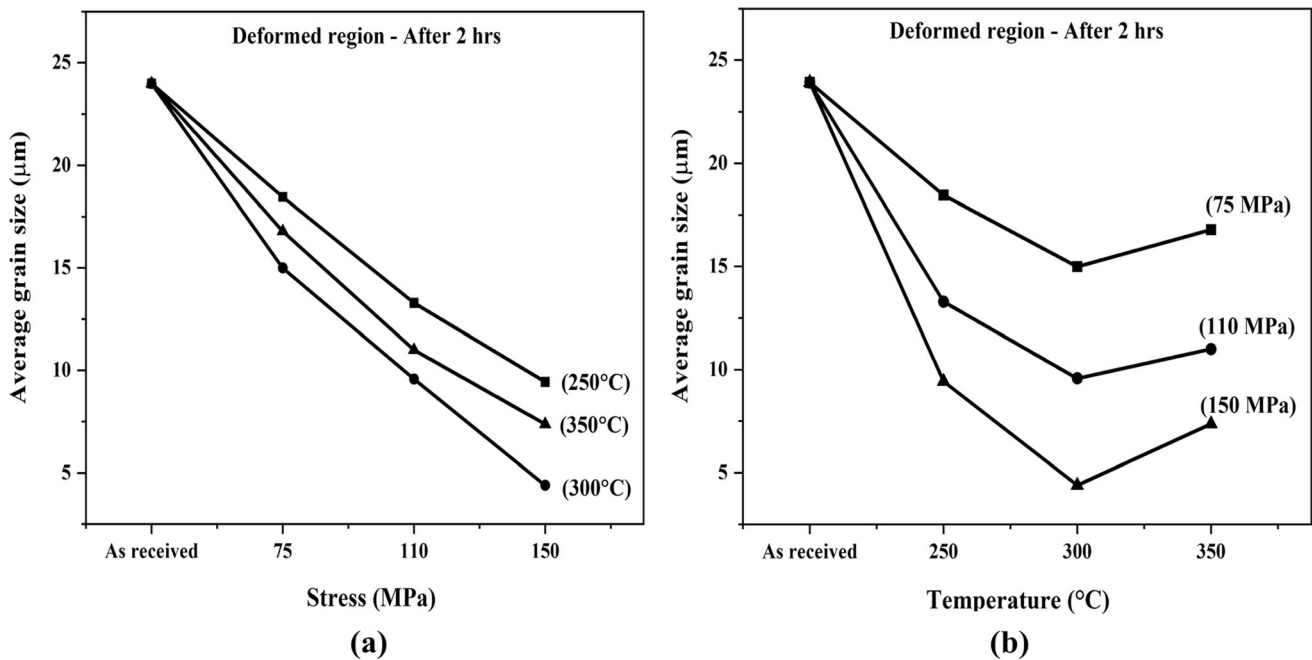
Fig. 6 Average grain size as a function of (a) Stress, MPa (b) Temperature (ºC).

Figure 2(a) shows the SEM image in the as-received state which also revealed the same. The average grain size was found to be 24 ± 1.2 μm. The average twin length and width were calculated to be 20 ± 1 and 5 ± 0.5 μm, respectively. It can be observed that the EDS study could confirm the presence of Cu & Zn (see Fig. 2b and c). Figure 3(a), (b) and (c) shows
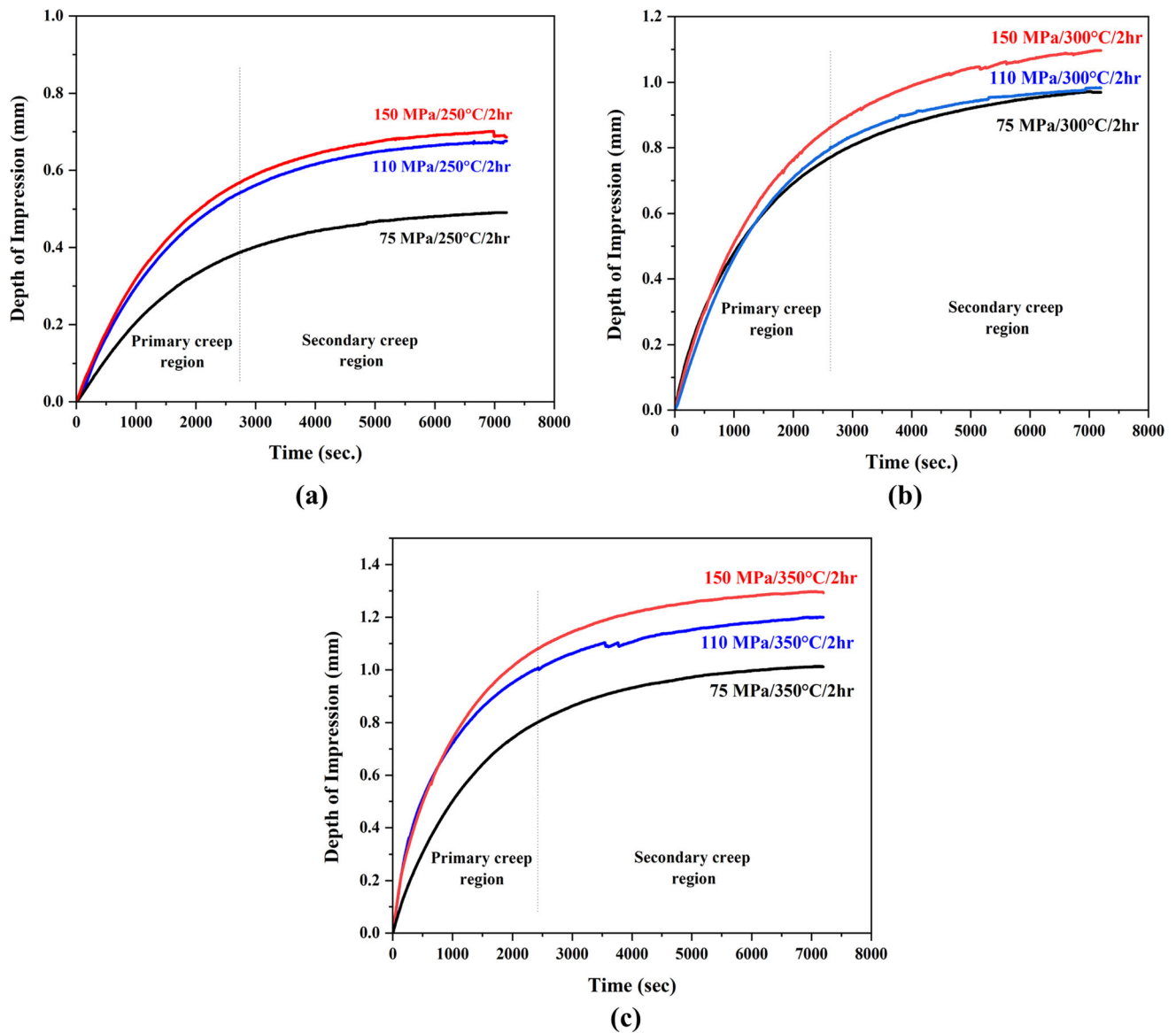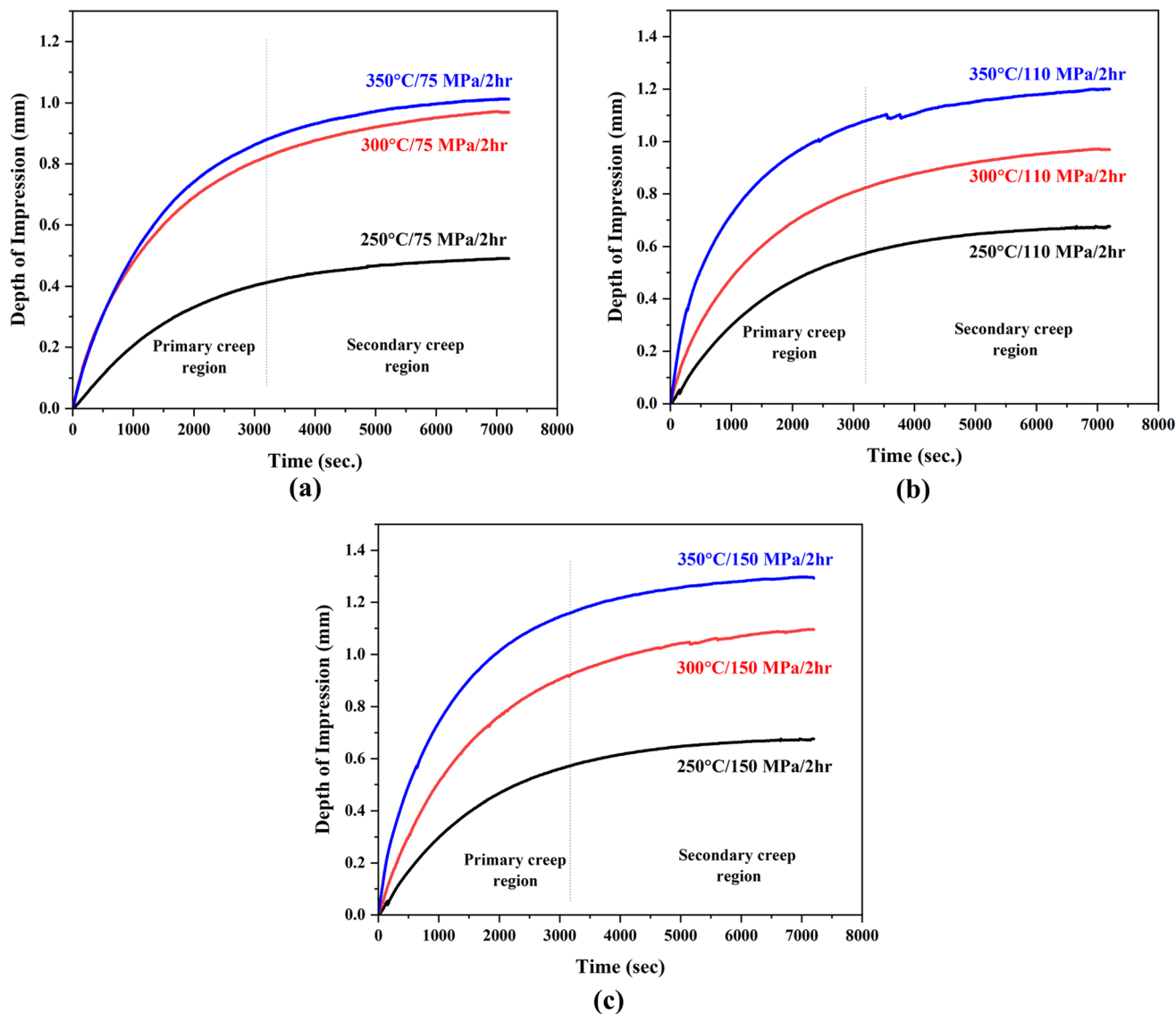
Fig. 7 Effect of load on the depth of impression with respect to time at various temperatures (a) 250ºC (b) 300ºC (c) 350ºC

SEM images of the impression or the deformed region of the samples tested at 250 °C and loads of 75, 110 and 150 MPa, respectively. Several twins and deformation bands are distinctly visible in the microstructures. Additionally, it was noticed that, at a constant temperature of 250 °C, an increase in the load results in a decrease in average grain size in the deformed region. Figure 4(a), (b) and (c) depicts SEM images of the deformed region at a constant load of 75 MPa at different temperatures of 250, 300 and 350 °C, respectively. It can also be observed that an increase in the test temperature also resulted in a negligible change in the grain size in the deformed region until 300 °C. However, for a temperature of 350 °C, the average grain size is found to increase slightly which might be due to the grain coarsening effect. The grain size in the undeformed (indenter non contact area) region increased on

increasing the temperature as observed in Fig. 5. Figure 6(a) gives a graphical representation of average grain size as a function of stress. It can be observed that with an increase in stress, the average grain size is found to decrease. Figure 6(b) depicts a graphical representation of average grain size as a function of temperature. It can be noted that there is a negligible change upon increasing the temperature from 250 to 350 °C.

3.2 Hot impression Creep Behavior

Figure 7(a), (b) and (c) gives the effect of load on the depth of impression with respect to time at various temperatures of 250, 300 and 350 °C, respectively. It can be observed that irrespective of the applied load and temperature, the depth of impression increases with an increase in time. When the load was increased from 75 to 150 MPa, the depth of impression

Fig. 8 Effect of temperature on the depth of impression with respect to time at various loads (a) 75 MPa (b) 110 MPa (c) 150 MPa

increased from 0.45 to 0.7 mm at 250 °C (see Fig. 7a), 0.9 to 1.1 mm at 300 °C (see Fig. 7b) and 1.0 to 1.3 mm at 350 °C (see Fig. 7c).

Thus, the higher the load for a given temperature, the higher the depth of impression obtained. The maximum depth of impression was observed at 150 MPa and 350 °C, whereas the minimum depth of impression was observed at 75 MPa and 250 °C. Figure 8(a), (b) and (c) gives the effect of temperature on the depth of impression with respect to time at various loads of 75, 110 and 150 MPa, respectively. When the deformation temperature was increased from 250 to 350 °C, the depth of impression increased from 0.45 to 1 mm at 75 MPa (see Fig. 8a), 0.7 mm to 1.2 at 110 MPa (see Fig. 8b) and 0.7 to 1.3 mm at 150 MPa (see Fig. 8c). Hence, the higher the

temperature for a given stress, the higher the depth of impression obtained as discussed by Yang et al. (Ref 22). The highest value of depth of impression of around 1.3 mm was obtained at 150 MPa/350 °C. Thus, one can say that both the load and testing temperature simultaneously affects the depth of impression. The higher the load and/or the temperature higher the impression depth formed, i.e., the higher the creep rate. Hence it is clear that the increase in depth of impression with an increase in temperature (at constant load) is much higher than that obtained with an increase in stress (at constant temperature). Thus, the effect of varying temperature on the depth of impression is much more dominant than that of the effect of varying the stress (Ref 17).
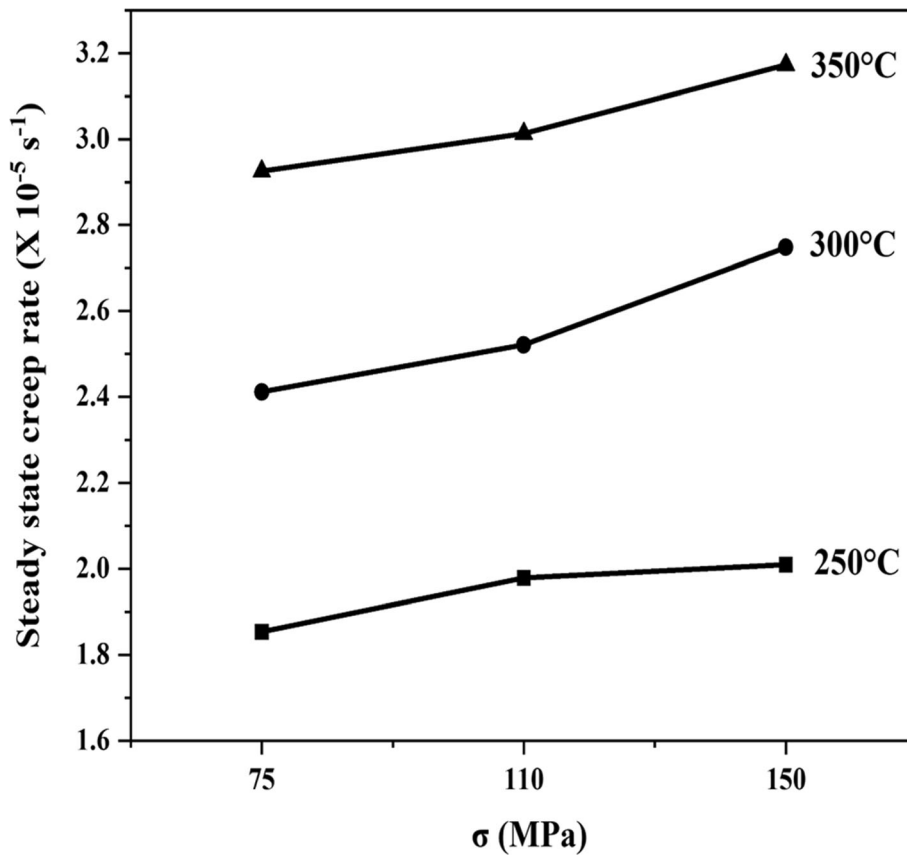
Fig. 9 Steady state creep rate (s^{-1}) vs. Stress (MPa)

Figure 9 gives the graphical plot of the steady-state creep rate as a function of stress. It can be noticed that irrespective of the test temperature, with an increase in the stress from 75 to 150 MPa, the steady state creep rate gradually increases. A similar trend was observed as a function of temperature while the stress remains constant. Hence this gives the information that with an increase in both temperature and stress, steady state creep rate increases progressively and these results go in hand with Sastry et al. (Ref 23). However, the effect of temperature on creep rate is more dominant than the effect of stress.

The Punch velocity vs time plot was obtained by differentiating the depth of impression vs time data at three different loads 75, 110 and 150 MPa as seen in Fig. 10(a), (b) and (c). It can be observed that, with an increase in time, the punch velocity decreases rapidly in the initial transient region and then gradually reaches a steady state. Upon increasing test temperature from 250 to 350 °C, the maximum punch velocity increased from 0.025 to 0.075 mm/min for a load of 75 MPa, i.e., the punch velocity increased nearly thrice, 0.015 to 0.07 mm/min for a load of 110 MPa, i.e., has increased more

than four times and 0.025 to 0.042 mm/min for a load of 150 MPa.

Additionally, the obtained punch velocity values were plotted with respect to (1/t), where t is the impression time in seconds. The curve obtained was then extrapolated to 1/t equals to zero. The corresponding punch velocity values obtained were taken to be the steady-state punch velocity values. Figure 11 gives a plot between steady-state velocity (mm/s) versus impression stress (MPa) at different test temperatures. Irrespective of the testing temperatures, an increment in the steady state velocity with respect to stress could be observed (Ref 24). However, the increase in steady-state velocity with respect to stress was drastic when the testing temperature was 350°C. Thus, it could be inferred that with an increase in temperature, the steady state punch velocity values also increased rapidly. This might be because of the decrease in strain hardening effect at higher temperatures and thus resulting in an increase in the displacement rate with an increase in temperature.
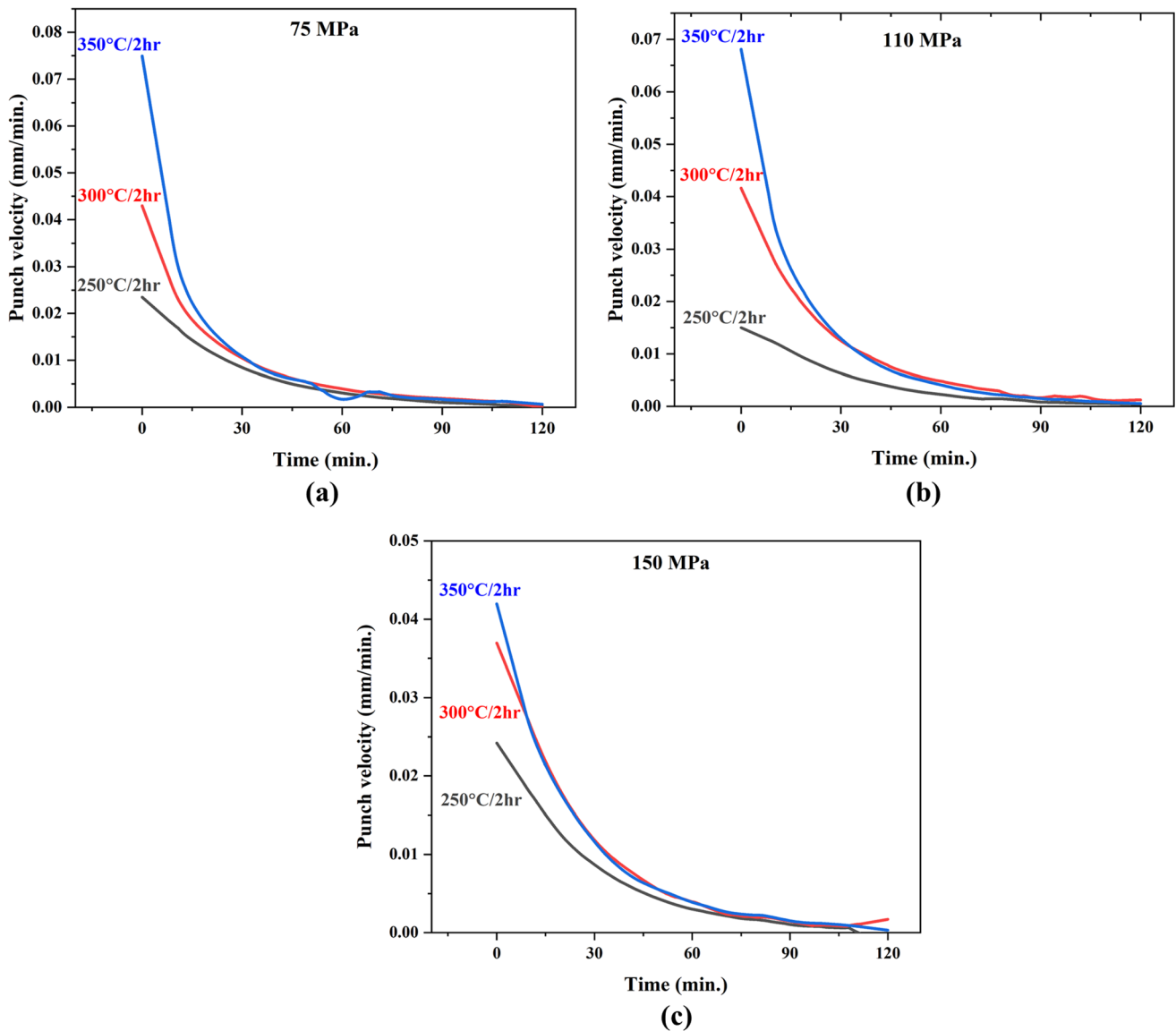
Fig. 10 Punch velocity (in mm/min) vs time (s) by varying temperatures at different loads (a) 75 MPa, (b) 110 MPa and (c) 150 MPa

3.3 Interpretation of Creep Mechanism

A double natural logarithm plot between the applied stress and steady-state punch velocity was plotted to get the stress exponent value, n. This stress exponent value obtained was further utilized in determining the activation energy. Further, a graph between $1000/T$ and $\ln[V_{imp} * T/G]0.17em- n \ln[\sigma_{imp}/G]$ was plotted to get the corresponding value of activation energy. With the stress exponent and activation energy values obtained, the impression creep mechanism responsible was predicted.

Figure 12 shows the plot between $\ln[V_{imp} * T/G]$ and $\ln[\sigma_{imp}/G]$ at temperatures 250, 300 and 350 °C. It can be observed that with an increase in the impression creep temperatures from 250 to 350 °C, the slope of the line obtained by plotting between $\ln[V_{imp} * T/G]$ and $\ln[\sigma_{imp}/G]$, i.e., stress exponent values decreased from 5.586 to 4.076. This trend in n values obtained goes in hand with the fact that lower deformation temperature and higher strain rate leads to the enhancement in the values of strain hardening exponent. The creep activation energy, Q values determined from plot between $1000/T$ and $\ln[V_{imp} * T/G]0.17em- n \ln[\sigma_{imp}/G]$ at various impression stress levels, is shown in Fig. 13. It can be observed that the creep activation energies at various deformation stress conditions 75, 110 and 150 MPa were 173, 165 and 153 kJ/mol, respectively, i.e., a decrease in activation energy with an increase in stress can be noticed. The average activation
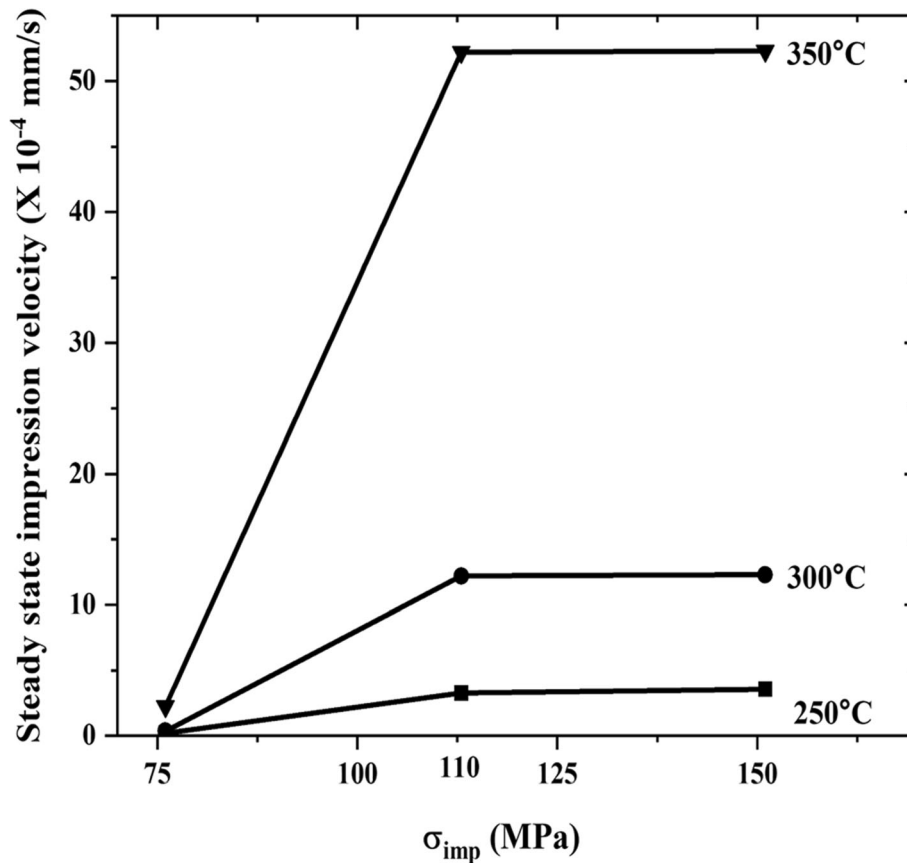
Fig. 11 Steady state velocity (mm/s) vs. impression stress (MPa)

energy value of the present Cu-1.5 Zn alloy was calculated to be 164 ± 10 kJ/mol

According to power law creep, various mechanisms have been attributed to different combinations of stress exponent, n and activation energy, Q values obtained. Dislocation flow and climb controls creep at lower temperatures and intermediate stresses while dislocation climb is the main factor that controls the creep rate. As stress rises, the stress exponent n for this mechanism of control may rise in the range of 2 to 7 (Ref 25, 26). In addition to it, at lower temperatures and intermediate stresses, the activation energy, Q is either the energy for lattice self-diffusion or the energy for pipe diffusion (Ref 27-29). The activation energy for lattice diffusion, Q_{ld} for copper has been reported to be 197 kJ/mol (Ref 30). Nevertheless, the reported activation energy for pipe diffusion, Q_{pd} for copper has been estimated to be between 118 and 157 kJ/mol (Ref 31).

Since the experimentally obtained stress exponent values for Cu-1.5 Zn alloy that is being studied at present, at different test temperatures lies between 4 and 5.5, dislocation climb is the responsible creep mechanism. However, considering all the impression stress conditions of 75, 110 and 150 MPa, the average activation energy value was found to be 164 ± 10 kJ/mol, which is much closer to the activation energy for pipe diffusion, Q_{pd} for copper. It could be concluded that the dislocation climb phenomenon controlled by dislocation pipe diffusion is exclusively responsible for creep in Cu-1.5 Zn alloy at temperature and stress ranges of 250 to 350 °C and 75 to 150 MPa, respectively.
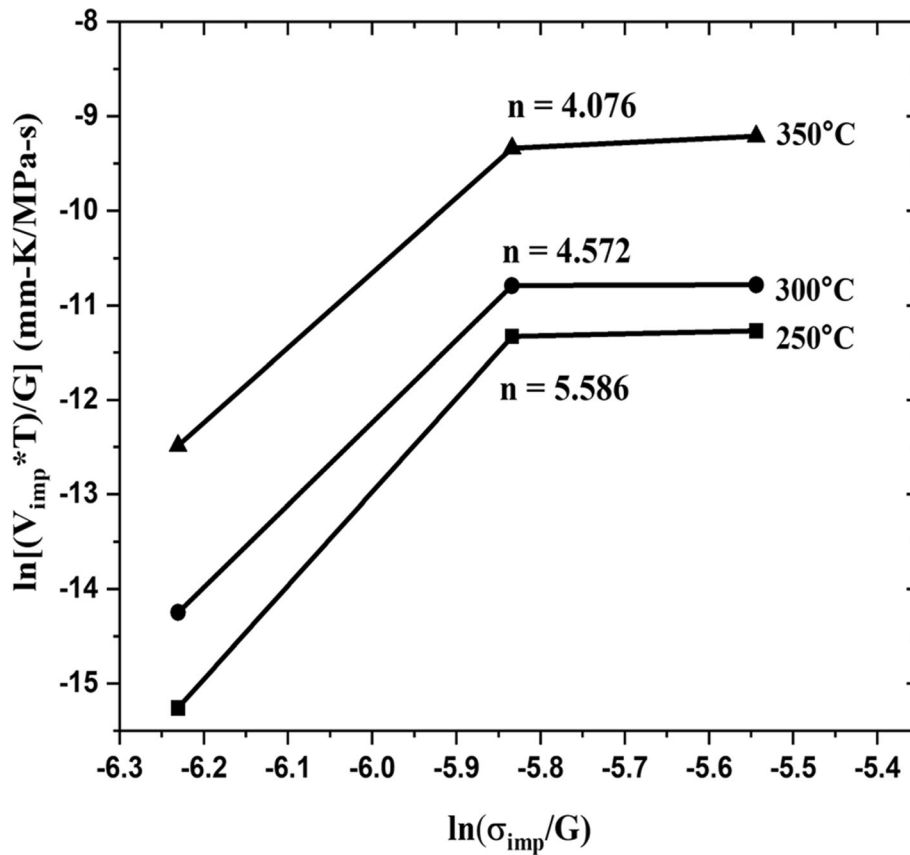
Fig. 12 Plot between $\ln[V_{imp} * T/G]$ and $\ln[\sigma_{imp}/G]$ at various temperatures for the determination of stress exponent, n

4. Conclusions

Impression creep test is a competent technique for analyzing the creep behavior of several material specimens. Based on the results obtained from the hot impression creep experiment conducted on the Cu-1.5 Zn alloy, the following conclusions can be drawn.

1. The microstructure of as received sample was found to consist of single-phase α grains. Several annealing twins and twin boundaries were also present in the microstructure.
2. Irrespective of the temperature and the load condition, the depth of impression increased with respect to the time. However, upon increasing the stress, more twins were observed. The influence of varying the temperature on the depth of impression is much more dominant than that of varying the stress.
3. Stress exponent lies between 4 and 5.5, whereas the average activation energy value was determined to be 164 ± 10 kJ/mol which is comparable to the activation energy for pipe diffusion of copper thereby, indicating that the dislocation climb phenomenon controlled by dislocation pipe diffusion as the controlling mechanism of the creep.
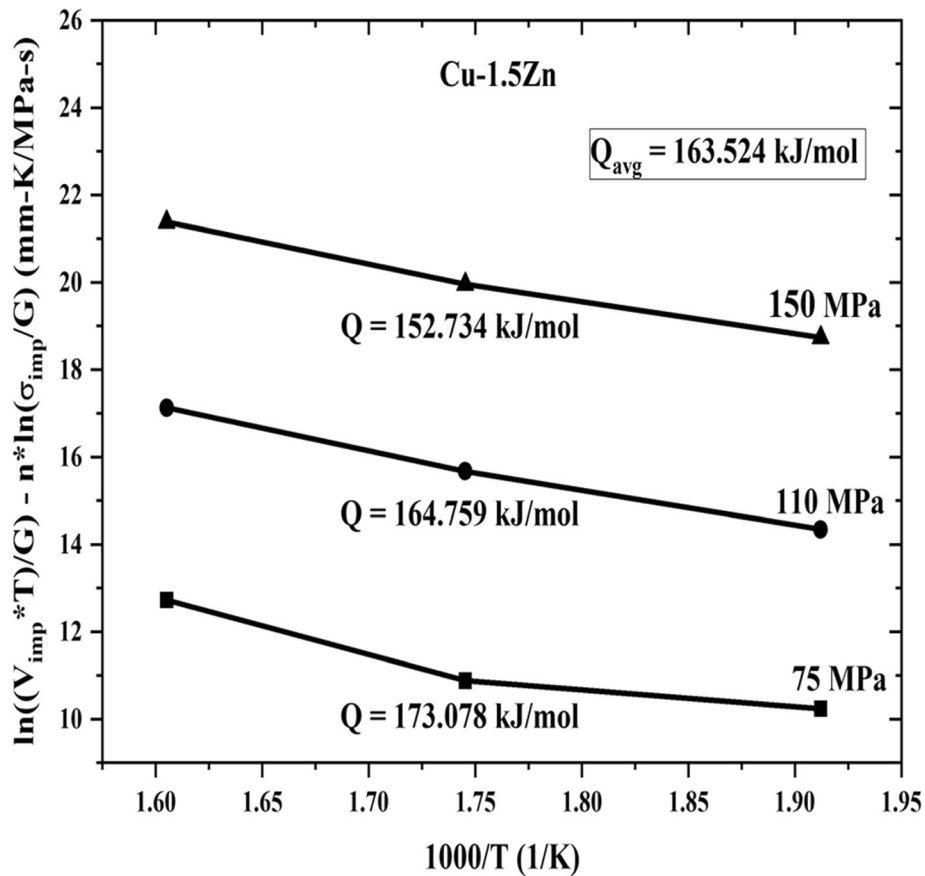
Fig. 13 Plot between 1000/T and $\ln[V_{imp} * T/G]0.17em- n\ln[\sigma_{imp}/G]$ at various stresses for determination of activation energy, Q

Acknowledgment

References

1. Copper Development Association Brass in Focus, 177, (2004), pp. 1–4, http://copperalliance.org.uk/docs/librariesprovider5/resources/pub-177-brass-in-focus-pdf.pdf?Status=Master&sfvrsn=0
2. A. Waheed and N. Ridley, Microstructure and Wear of Some High-Tensile Brasses, *J. Mater. Sci.*, 1994, **29**, p 1692–1699
3. M.R. Willis and J.P. Jones, Creep Mechanisms is Dual Phase Brass, *Scripta Mater.*, 2001, **44**, p 31–36
4. S.V. Garimella, A.S. Fleischer, J.Y. Murthy, A. Keshavarzi, R. Prasher, and C. Patel, Thermal Challenges in Next-Generation Electronic Systems, *IEEE Trans. Compon. Packag. Technol.*, 2008, **31**(4), p 801–815
5. K. Puttaswamy and G.H. Loh, Thermal Analysis of a 3D Die-stacked High-Performance Microprocessor. *Proceedings of the 16th ACM Great Lakes symposium on VLSI*, 2006, Philadelphia. ACM, New York, 2006, p 19–24
6. K. Zhang, J.R. Weertman, and J.A. Eastman, The Influence of Time, Temperature, and Grain Size on Indentation Creep in High-Purity Nanocrystalline and Ultrafine Grain Copper, *Appl. Phys. Lett.*, 2004, **85**(22), p 5197–5199
7. F. Sket, A. Isaac, K. Dzieciol, G. Sauthoff, A. Borbély, and A.R. Pyzalla, In situ Tomographic Investigation of Brass During High-Temperature Creep, *Scripta Mater.*, 2008, **59**(5), p 558–561
8. J. A. La Manna Jr., Doctoral thesis on A Study of the Relationship between Indentation Creep and Uniaxial Creep. University of Tennessee, Knoxville
9. W. Yan, S. Wen, J. Liu, and Z. Yue, Comparison Between Impression Creep and Uni-axial Tensile Creep Performed on Nickel-Based Single Crystal Superalloys, *Mater. Sci. Eng. A*, 2010, **527**, p 1850–1855
10. H.Y. Yu, M.A. Imam, and B.B. Rath, Study of the Deformation Behaviour of Homogeneous Materials by Impression Tests, *J. Mater. Sci.*, 1985, **20**, p 636–642
11. V.R. Rao, D.K. Pattanayak, and C. Vanitha, Hot Impression Creep Behavior of AlSi10Mg Alloy Fabricated through SLM Route, *Trans. Indian Inst. Metals*, 2022, **76**(2), p 271–277
12. P. Bharath Sreevatsava, E. Vara Prasad, A. Sai Deepak Kumar, M.F. Anwar, V.R. Rao, and V. Chilamban, Effects of Temperature and Load during Hot Impression Behavior of Cr-Ni Stainless Steel, *Metall. Mater. Eng.*, 2021, **27**(4), p 531–539
13. K. Kuchařová, F. Dobeš, A. Orlová, K. Milička, and J. Čadek, High Temperature Creep in Precipitation Strengthened Cu-2Fe Alloy, *Metal Sci.*, 1984, **18**(3), p 137–142
14. A. Akbari-Fakhrabadi, R. Mahmudi, A.R. Geranmayeh, and M. Jamshidijam, Impression Creep Behaviour of a Cu-6Ni-2Mn-2Sn-2Al Alloy, *Mater. Sci. Eng. A*, 2012, **535**, p 202–208
15. R. Mahmudi, A. Karsaz, A. Akbari-Fakhrabadi, and A.R. Geranmayeh, Impression Creep Study of a Cu-0.3Cr-0.1Ag Alloy, *Mater. Sci. Eng. A*, 2010, **527**, p 2702–2708
16. R. Mahmudi, A. Akbari-Fakhrabadi, A. Karsaz, and A.R. Geranmayeh, Creep Behavior of Copper and Cu-0.3Cr-0.1Ag Alloy, *J. Eng. Mater. Technol.*, 2010, **132**, p 044501–044511
17. S.D. Kumar, M.F. Anwar, E. Vara Prasad, P. Bharath Sreevatsava, and C. Vanitha, Effect of Temperature and Load during Hot Impression Creep of Cu-Zn-Al Alloy, *Mater. Today Proc.*, 2021, **39**, p 1296–1302
18. Proc. 2nd Int. Conf. on Creep and Fracture of Engineering Materials and Structures, Pineridge Press Ltd., Swansea, (1984) pp. 235
19. S.I. Shakil, A. Hadadzadeh, H. Pirgazi, M. Mohammadi, and M. Haghshenas, Indentation-derived Creep Response of Cast and Laser Powder Bed Fused AlSi10Mg Alloy: Air Temperature, *Micron*, 2021, **150**, p 103145

20. S.N. Chu and J.C.M. Li, Impression Creep; A New Creep Test, *J. Mater. Sci.*, 1977, **12**, p 2200–2208

21. S.V. Raj and T.G. Langdon, Creep Behaviour of Copper at Intermediate Temperatures-I. Mechanical Characteristics, *Acta Metall.*, 1989, **37**, p 843–852

22. F. Yang and J.C.M. Li, Impression and Diffusional Creep of Anisotropic Media, *J. Appl. Phys.*, 1995, **77**(1), p 110–117

23. D.H. Sastry, Impression Creep Technique-An Overview, *Mater. Sci. Eng. A*, 2005, **409**(1–2), p 67–75

24. S. Li, D. Purdy, S.J. Brett, D. Deng, A. Shibli, and W. Sun, Effect of Indentation Depth in Impression Creep Test: Conversion Relationships and Correction Functions, *Mater. High Temp.*, 2021, **38**(5), p 358–367

25. T.G. Langdon, Identifiying Creep Mechanisms at Low Stresses, *Mater. Sci. Eng. A*, 2000, **283**, p 266–273

26. W. H. Bowyer, Creep of the Copper Canister-A Critical Review of the Literature. SKI report 2003:23, Meadow End Farm, Tilford, Farnham, Surrey, GU10 2DB, England, April 2003

27. M.D. Mathew, H. Yang, S. Movva, and K.L. Murty, Creep Deformation Characteristics of Tin and Tin-Based Electronic Solder Alloys, *Metall. Mater. Trans. A*, 2005, **36**, p 99–105

28. S.S. Vagarali and T.G. Langdon, Deformation Mechanisms in hcp Metals at Elevated Temperatures—I. Creep Behaviour of Magnesium, *Acta Metall.*, 1981, **29**(12), p 1969–1982

29. B. Sivaiah and S.P. Gupta, Diffusion Induced Grain Boundary Migration in the Cu-Zn System, *Mater. Charact.*, 2008, **59**(9), p 1141–1151

30. H.J. Frost and M.F. Ashby, *Deformation-Mechanism Maps, the Plasticity and Creep of Metals and Ceramics*, Pergamon, Oxford, UK, 1982, p 21

31. J.P. Poirier, *Creep of Crystals, High Temperature Deformation Processes in Metals, Ceramics, and Minerals*, Cambridge University Press, New York, 1985